Multi-objective Optimization of Integrated Energy Systems Considering Ladder-type Carbon Emission Trading and Refined Load Demand Response

Yanhong Luo, *Member*, *IEEE*, Haowei Hao, Dongsheng Yang, *Senior Member*, *IEEE*, and Bowen Zhou, *Member*, *IEEE*

***Abstract*—In this paper, a novel multi-objective optimization model of integrated energy systems (IESs) is proposed based on the ladder-type carbon emission trading mechanism and refined load demand response strategies. First, the carbon emission trading mechanism is introduced into the optimal scheduling of IESs, and a ladder-type carbon emission cost calculation model based on rewards and penalties is established to strictly control the carbon emissions of the system. Then, according to different response characteristics of electric load and heating load, a refined load demand response model is built based on the price elasticity matrix and substitutability of energy supply mode. On these basis, a multi-objective optimization model of IESs is established, which aims to minimize the total operating cost and the renewable energy source (RES) curtailment. Finally, based on typical case studies, the simulation results show that the proposed model can effectively improve the economic benefits of IESs and the utilization efficiency of RESs.**

***Index Terms*—Integrated energy system, carbon emission trading, load demand response, renewable energy source.**

I. Introduction

DUE to the rapid development of economy, the utilization of fossil energy has resulted in many serious problems such as the depletion of traditional energy resources and the deterioration of global climate [1]. Therefore, the active development and rational use of renewable energy sources (RESs) has become an inevitable choice to solve the problems. The integrated energy system (IES) can coordinate the management of electric energy, heat energy, natural gas, and a variety of RESs and significantly improve the utilization of clean energy [2], [3].

As an important carrier of RES utilization, there have been a lot of research on multi-energy systems. In [4], an optimal scheduling framework of the industrial IES is proposed, which synchronously coordinates the energy generation, conversion, storage, and trading to reduce energy costs in industrial environments. In [5], a transaction scheme of internal energy sharing in microgrids is proposed to decrease the transaction with external energy networks, so as to realize the effect of reducing the operating cost of the whole grids. The heat storage (HS) tanks are configured to decouple electricity-heat, achieving the improvement of the RES accommodation capability of the system in [6], [7]. In [8], the energy hub that integrates heat pumps and combined cool, heat, and power units with RESs is considered to improve the complementarity of multiple energy and the economy of energy hub. However, the above studies only consider the overall economic benefits of the system, while ignoring the influence of carbon emissions on the environment and system operation.

Carbon emission trading mechanism can make carbon emission rights become a schedulable resource with economic value, so as to realize the economic and low-carbon development of the energy system. In [9], the economy and energy efficiency of IESs with carbon emission trading mechanism are analyzed, and the result indicates that the implementation of carbon emission trading scheme can significantly promote carbon reduction and operation optimization. In [10] and [11], the traditional carbon emission trading model, i.e., the unified carbon emission cost calculation model is applied to the optimal scheduling of multi-energy system. However, the calculation model of carbon emission trading cost is not improved and the modeling of carbon emission trading cost is too simple. The ladder-type carbon emission trading mechanism is a policy tool to deal with climate change, which aims to achieve effective control of carbon emissions. In [12] and [13], based on traditional carbon emission trading mechanism, a ladder-type carbon emission trading model is built and an optimal scheduling model of electricity-heat-gas IES is also proposed. But in [12] and [13], the modeling

Manuscript received: April 14, 2023; revised: June 1, 2023; accepted: August 26, 2023. Date of CrossCheck: August 26, 2023. Date of online publication: October 13, 2023.

This work was supported by the Science and Technology Project of State Grid Corporation of China "Key Technologies and Application of Distributed Swarm Intelligent Collaborative Control and Optimization for Energy Internet" (No. 52100220002B).

Y. Luo (corresponding author), H. Hao, D. Yang, and B. Zhou are with the Department of Electric Engineering, Northeastern University, Shenyang 110004, China (e-mail: luoyanhong@ise.neu.edu.cn; 254411619@qq.com; yangdongsheng@ise.neu.edu.cn; zhoubowen@ise.neu.edu.cn).

DOI: 10.35833/MPCE.2023.000230

of carbon emission trading cost model is not detailed enough. And the carbon emission modeling of devices in the system is not comprehensive enough, and the impacts of some devices on the total carbon emissions is not taken into account. In addition, for the above studies, the demand response is not considered, resulting in the regulating effect on user side cannot be brought into full play.

Load demand response (LDR) can effectively promote the adjustment of energy consumption behaviors of users through the energy price and economic incentive mechanism [14]. The authors in [15] propose an optimization model that includes LDR program based on incentive into the energy management of microgrid, which aims to maximize the rewards provided to the users participating in LDR. In [16] and [17], the LDR based on the time-sharing electricity price is applied to the scheduling of energy hub, and the system is encouraged to coordinate various forms of energy to conserve energy consumption. But only the demand response of electric load is taken into account in [16], [17], and other forms of energy load are not considered in the demand response. In [18], a joint optimal operation model considering the demand response of both power and heating load on the user side is established to meet the energy demand of users and improve the utilization of wind power, but the modeling methods of LDR are relatively simple. The flexible load resource model is built and further used to the optimal dispatch of IESs in [19]. On the premise of meeting constraints of consumer satisfaction, the regulation role of flexible resources participating in LDR can be brought into full play. However, the classification of flexible resources involved in LDR is not refined enough, and the modeling of heating flexible resources and the substitution relationship between different forms of energy load are simplified. Besides, the above studies only consider single objective optimization, which have difficulty in coordinating multiple scheduling requirements.

In view of the above problems, this paper proposes a novel multi-objective optimization model of IESs, which considers both the ladder-type carbon emission trading mechanism and the refined LDR strategies. The main contributions are summarised as follows.

1) The carbon emission trading mechanism is introduced into the optimal scheduling of IESs. The impacts of each device on carbon emissions are fully considered, and a ladder-type carbon emission cost calculation model based on reward and penalty is built to strictly control the carbon emissions and reduce the carbon trading cost of IESs.

2) According to different flexible characteristics and scheduling potential of load, a refined LDR model based on the price elasticity matrix and the mutual conversion of electric load and heating load on the energy consumption side is established, so as to fully utilize the regulation role of flexible resources.

3) A multi-objective optimization model of IES is established to minimize the total operating cost and the RES curtailment. And the simulation results of the examples verify the effectiveness and superiority of the model proposed in this paper.

The remainder of this paper is organized as follows. The structure of IES is introduced and the mathematical models are established in Section II. Section III builds the multi-objective optimization model of IES and the solution method is also introduced. Case studies are presented in Section IV. Finally, the main conclusions are drawn in Section V.

II. Structure and Modeling of IESs

A. Structure of IESs

The IES can achieve complementarity and coordination of multiple energy sources and ensure continuous and reliable energy supply. The structure of the IES in this paper is shown in Fig. 1. For the IES, the input side is connected to the external power grid and natural gas grid, respectively. And the electric energy is also supplied by wind turbine (WT) and photovoltaic (PV). The output side is connected to the users on the demand side to meet the electricity demand and heating demand of users. On the energy conversion side, the electricity and natural gas are converted into other forms of energy through the combined heat and power (CHP) unit, gas boiler (GB), and power to gas (P2G) unit. The CHP unit is composed by a micro-gas turbine (MT) and a heat recovery boiler (HRB). The MT is used to generate electricity, and the HRB can absorb the waste heat from the MT and supply it to users. In addition, the electricity storage (ES) device, heat storage (HS) device, and gas storage (GS) device are added into the IES, which makes the energy controllable and effectively improves the operation efficiency.

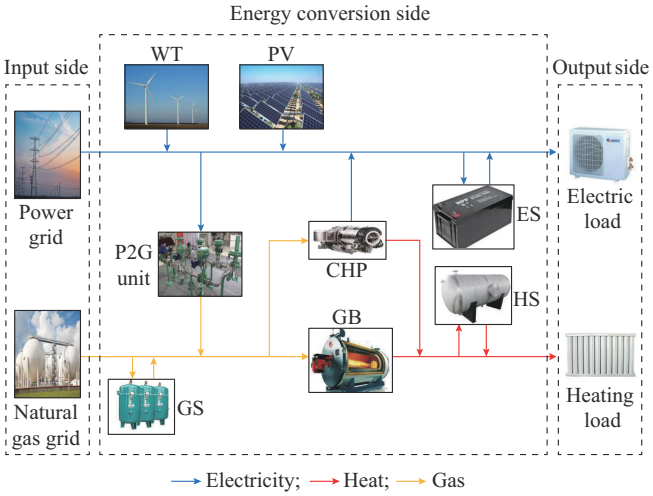

Fig. 1. Structure of IES.

B. Modeling of Energy Storage Devices

1) ES Model

The ES is an important part of the IES. In [20] and [21], on the basis of traditional lithium-ion battery model and lead-acid battery model, a modified battery model is proposed. Based on practical experience, the efficiency of a battery is decided by its physical state. According to [22], the main source of power loss in lead-acid and lithium-ion batteries

arises from heat loss during their charging or discharging processes. This heat is produced by the ohmic resistance within the electrodes and electrolytes, as well as polarization effects. The degree of power loss is proportional to the voltage drop (polarization) caused by the flow of current. According to [23], the lead-acid and lithium-ion batteries exhibit same characteristics at the end of their charging cycles, because the voltage increases rapidly when being fully charged. The polarization resistance term can be used to model this phenomenon. So the voltage drop of the lead-acid and lithium-ion batteries can be obtained according to the empirical approach in [23]. Therefore, the consumption during charging and discharging processes of lead-acid and lithium-ion batteries can be expressed as:

$$C_t^{bat}=\frac{10^3 C_r K(1-SOC_t)}{V_r^2\cdot SOC_t}P_t^{bat,c}+\frac{10^3\left(R_{in}+\dfrac{K}{1.1-SOC_t}\right)}{V_r^2}(P_t^{bat,c})^2 \tag{1}$$

$$D_t^{bat}=\left[\frac{10^3 C_r K(1-SOC_t)}{V_r^2\cdot SOC_t}+1\right]P_t^{bat,d}+\frac{10^3\left(R_{in}+\dfrac{K}{SOC_t}\right)}{V_r^2}(P_t^{bat,d})^2 \tag{2}$$

where C_t^{bat} is the power consumption of the battery during charging process in time period t, which is equivalent to the charging loss; D_t^{bat} is the power consumption of the battery during discharging process in time period t, which is equivalent to the sum of actual discharging power and discharging loss; SOC_t is the state of charge (SOC) of the battery; R_{in} is the internal resistance of the battery; K is the battery polarization constant that can be calculated according to the manufacturer's data; C_r and V_r are the rated capacity and rated voltage of the battery, respectively; and $P_t^{bat,c}$ and $P_t^{bat,d}$ are the charging and discharging power of the battery, respectively.

Thus, the SOC of the battery can be represented as:

$$SOC_t=SOC_{t-1}+\frac{P_t^{bat,c}-C_t^{bat}}{W^{bat,\max}}\quad P_t^{bat,c}>0 \tag{3}$$

$$SOC_t=SOC_{t-1}-\frac{D_t^{bat}}{W^{bat,\max}}\quad P_t^{bat,d}>0 \tag{4}$$

where $W^{bat,\max}$ is the maximum ES capacity of the battery.

Besides, the actual output power of the battery is:

$$P_t^{bat}=P_t^{bat,d}-P_t^{bat,c} \tag{5}$$

The maintenance cost of the battery can be expressed by a linear function of its charging and discharging power consumption [21]:

$$C_t^{ES}=\begin{cases}c_{bat}C_t^{bat}\Delta t & C_t^{bat}>0\\ c_{bat}D_t^{bat}\Delta t & D_t^{bat}>0\end{cases} \tag{6}$$

where c_{bat} is the unit maintenance cost of the battery consumption.

2) HS and GS Models

When the heat energy generated by CHP and GB cannot be fully absorbed, it can be temporarily stored in HS and released when the heating demand is high, which realizes the transfer of heat energy in time and raises the utilization of heat energy. Similarly, the excess natural gas generated by P2G can be stored into the GS. The mathematical models of HS and GS can be represented as:

$$W_t^{HS}=W_{t-1}^{HS}+H_t^{ch}\eta_{ch}\Delta t-\frac{H_t^{dis}\Delta t}{\eta_{dis}} \tag{7}$$

$$W_t^{GS}=W_{t-1}^{GS}+Q_t^{ch}\mu_{ch}\Delta t-\frac{Q_t^{dis}\Delta t}{\mu_{dis}} \tag{8}$$

where W_t^{HS} and W_t^{GS} are the stored heat energy of HS and the stored natural gas of GS, respectively; H_t^{ch} and H_t^{dis} are the heat storing power and heat releasing power of HS, respectively; η_{ch} and η_{dis} are the heat storing efficiency and heat releasing efficiency of HS, respectively; Q_t^{ch} and Q_t^{dis} are the gas storing power and gas releasing power, respectively; and μ_{ch} and μ_{dis} are the input efficiency and output efficiency of GS, respectively.

From above, the actual output power of HS and GS can be represented as:

$$H_t^{HS}=H_t^{dis}-H_t^{ch} \tag{9}$$

$$Q_t^{GS}=Q_t^{dis}-Q_t^{ch} \tag{10}$$

C. Carbon Emission Trading Mechanism Model

The carbon emission trading mechanism refers to the establishment of legal carbon emission rights and allowing them to be traded on the carbon market, which is intended to control carbon emissions. The free carbon emission credits are allocated to the carbon emission sources of energy suppliers by the government firstly. If the carbon emission credits are exceeded by the carbon emissions in the actual production process, the energy suppliers need to buy additional carbon emission credits in the carbon trading market. If the carbon emissions of energy suppliers are lower than their existing emission credits, according to the carbon trading price of the day, i.e., unit carbon emission price, the excess carbon emission credits can be sold on the carbon market, so as to gain certain benefits.

1) Allocation of Initial Carbon Emission Credits

In this paper, the distribution of initial carbon emission credits in IES consists of three parts: electricity purchased from external power grid, CHP, and GB. CHP can generate electric power and heat power by MT and HRB, respectively. According to the "Shanghai 2016 Carbon Emission Allocation Scheme", the electricity generated by CHP can be transformed into equivalent heat. Based on this, the carbon emission credit allocation of CHP is determined by the equivalent heat generation. Therefore, the expression of free carbon emission credits of IES is:

$$E^F=E^{grid}+E^{CHP}+E^{GB} \tag{11}$$

$$E^{grid}=P_t^{grid}\varepsilon_p \tag{12}$$

$$E^{CHP}=(H_t^{HRB}+\delta P_t^{MT})\varepsilon_h \tag{13}$$

$$E^{GB}=H_t^{GB}\varepsilon_h \tag{14}$$

$$H_t^{HRB}=\frac{\eta_{HRB}(1-\eta_{MT})P_t^{MT}}{\eta_{MT}} \tag{15}$$

where E^F is the initial carbon emission credit; E^{CHP}, E^{GB}, and E^{grid} are the carbon emission credits of CHP, GB, and electricity purchased from the power grid, respectively; P_t^{grid} is the electric power purchased from the grid; ε_p is the carbon emission credit per unit of electricity supply; P_t^{MT} and H_t^{HRB} are the electric power generated by MT and the heat power recovered by HRB, respectively; δ is the transformation coefficient from electricity to heat of CHP; η_{HRB} is the recovery efficiency of HRB; η_{MT} is the electricity generation efficiency of MT; ε_h is the carbon emission credit per unit of heat supply; and H_t^{GB} is the heat power output by GB.

2) Ladder-type Carbon Emission Cost Calculation Model Based on Rewards and Penalties

In the actual energy supply process, the consumptions of electricity and natural gas decide the carbon emissions of the whole energy system. Besides, for P2G, CO_2 is required to be used as raw materials in the process of converting electricity to gas. And we think that CO_2 consumed by P2G also participates in the carbon trading. Therefore, the actual carbon emissions of IES can be expressed as:

$$E^A = P_t^{grid}\varepsilon_e + (F_t^{MT} + F_t^{GB} - F_t^{P2G})\varepsilon_g \tag{16}$$

$$F_t^{MT} = \frac{P_t^{MT}}{\eta_{MT}\lambda_{gas}} \tag{17}$$

$$F_t^{GB} = \frac{H_t^{GB}}{\eta_{GB}\lambda_{gas}} \tag{18}$$

$$F_t^{P2G} = \frac{P_t^{P2G}\eta_{P2G}}{\lambda_{gas}} \tag{19}$$

where E^A is the actual carbon emission; ε_e and ε_g are the unit carbon emission coefficients of electricity consumption and natural gas consumption, respectively; F_t^{MT} is the gas consumed by MT; λ_{gas} is the calorific value of natural gas; F_t^{GB} is the gas consumed by GB; η_{GB} is the heat production efficiency of GB; F_t^{P2G} is the gas absorbed by P2G; P_t^{P2G} is the electric power consumed by P2G; and η_{P2G} is the electricity-gas conversion efficiency of P2G.

On the basis of the conventional carbon emission trading mechanism, this paper proposes a ladder-type carbon emission cost calculation model based on rewards and penalties. Based on initial carbon emission credits, several emission ranges are divided. When $E^A < E^F$, the incentive factor is introduced. It means that in addition to selling excess carbon emission credits on the carbon trading market for profit, the government will also give some incentives to energy suppliers. And the smaller the carbon emission range corresponding to carbon emissions, the more incentives the government will give and the more benefits can be obtained. Conversely, when $E^A > E^F$, the greater the emission range corresponding to carbon emissions, the higher the carbon trading price, which means that more carbon emission cost penalties are imposed on energy suppliers. These policies on the division of carbon emission ranges are formulated by the government. The ladder-type carbon emission trading cost of IES can be calculated by:

$$C_{co_2} = \begin{cases} F_{co_2}(1+2\gamma)(E^A - E^F + d) & E^A \le E^F - d \\ F_{co_2}(1+\gamma)(E^A - E^F) - F_{co_2}(1+2\gamma)d & \\ & E^F - d < E^A \le E^F \\ F_{co_2}(E^A - E^F) & E^F < E^A \le E^P \\ F_{co_2}(1+\rho)(E^A - E^P) + F_{co_2}(E^A - E^F) & \\ & E^P < E^A \le E^P + d \\ F_{co_2}(1+2\rho)(E^A - E^P - d) + F_{co_2}(1+\rho)d + F_{co_2}(E^A - E^F) & \\ & E^P + d < E^A \le E^P + 2d \\ F_{co_2}(1+3\rho)(E^A - E^P - 2d) + F_{co_2}(1+2\rho)d + & \\ \quad F_{co_2}(1+\rho)d + F_{co_2}(E^A - E^F) & E^P + 2d < E^A \end{cases} \tag{20}$$

where F_{co_2} is the carbon price in carbon emission trading market; γ is the incentive factor; d is the interval length of carbon emission range; E^P is the target value of carbon reduction; and ρ is the extent of carbon price growth for each ladder. It should be mentioned that when the proposed carbon emission cost calculation model is applied to practice, the government can establish the standard of carbon emission interval length according to the actual situation and demand, so as to realize the goal of carbon emission reduction.

Through the ladder-type carbon emission trading mechanism, the high-emission energy suppliers need to pay higher carbon emission costs, which encourages them to reduce emissions and promotes a shift towards low-carbon and environmentally friendly development models. At the same time, the energy suppliers with low emissions can reduce operating costs and have an advantage in the market. Therefore, the ladder-type carbon emission trading mechanism has attracted the attention of many academic researchers. Even if the ladder-type carbon emission trading mechanism has not been widely applied in current carbon trading market, its wide popularization is an inevitable trend in the future.

D. Refined LDR Model

The traditional LDR model usually only considers the demand response of electric load, for example, changing the user's electricity consumption habits by adjusting the price of electricity. However, in IES, there are other load forms. So not only electric load can be involved in LDR, but also the heating load can participate in LDR regulation. Therefore, the LDR model proposed in this paper considers the demand response of both electric and heating loads, so as to fully utilize flexible resources. In view of the load characteristics of the user side, the loads in IES can be divided into uncontrollable load (UL) and controllable load (CL). And the LDR in this paper divides CL into price dependent load (PDL) and energy fungible load (EFL).

1) PDL Model

The sensitivity of different types of load to energy price signal is different. Therefore, PDL can be further divided into time transferable load (TTL) and quantity reducible load (QRL).

1) TTL model

TTL means that the users take the time-sharing energy price as the signal, some loads during peak period of energy consumption are shifted to low peak period, and the total TTL remains unchanged during the scheduling cycle. According to the ratio of time-sharing energy price to initial energy price, the TTL characteristics can be described by price demand elasticity matrix $\boldsymbol{E}_{TTL}(i,j)$:

$$\boldsymbol{E}_{TTL}(i,j)=\begin{bmatrix} e_{11}^{TTL} & e_{12}^{TTL} & \cdots & e_{1j}^{TTL} \\ e_{21}^{TTL} & e_{22}^{TTL} & \cdots & e_{2j}^{TTL} \\ \vdots & \vdots & & \vdots \\ e_{i1}^{TTL} & e_{i2}^{TTL} & \cdots & e_{ij}^{TTL} \end{bmatrix} \tag{21}$$

$$e_{ij}^{TTL}=\frac{\Delta P_i^{TTL}}{P_i^{TTL,0}}\left(\frac{\Delta\phi_j}{\phi_j^0}\right)^{-1} \tag{22}$$

where e_{ij}^{TTL} is the element of the price demand elasticity matrix of TTL; $P_i^{TTL,0}$ is the initial TTL in time period i; ϕ_j^0 is the initial energy price in time period j; ΔP_i^{TTL} is the variation of TTL after LDR in time period i; and $\Delta\phi_j$ is the variation of energy price after LDR in time period j.

Thus, the variation of TTL can be further represented as:

$$\Delta P_i^{TTL}=P_i^{TTL,0}\sum_{j=1}^{T}\frac{e_{ij}^{TTL}\Delta\phi_j}{\phi_j^0} \tag{23}$$

To ensure the total TTL remains unchanged before and after LDR, the following condition should be met:

$$\sum_{i=1}^{T}\Delta P_i^{TTL}=0 \tag{24}$$

2) QRL model

QRL represents that in order to relieve scheduling pressure, the load is reduced in peak period of energy consumption. And the price demand elasticity matrix of QRL is represented as diagonal matrix $\boldsymbol{E}_{QRL}(i,j)$:

$$\boldsymbol{E}_{QRL}(i,j)=\begin{bmatrix} e_{11}^{QRL} & 0 & \cdots & 0 \\ 0 & e_{22}^{QRL} & \cdots & 0 \\ \vdots & \vdots & & \vdots \\ 0 & 0 & \cdots & e_{ij}^{QRL} \end{bmatrix} \tag{25}$$

$$e_{ij}^{QRL}=\frac{\Delta P_i^{QRL}}{P_i^{QRL,0}}\left(\frac{\Delta\phi_j}{\phi_j^0}\right)^{-1} \tag{26}$$

where e_{ij}^{QRL} is the element of the price demand elasticity matrix of QRL; and $P_i^{QRL,0}$ and ΔP_i^{QRL} are the initial QRL and the variation of QRL after LDR, respectively.

Therefore, the variation of QRL can be calculated by:

$$\Delta P_i^{QRL}=P_i^{QRL,0}\sum_{j=1}^{T}\frac{e_{ij}^{QRL}\Delta\phi_j}{\phi_j^0} \tag{27}$$

2) EFL Model

EFL means that part of the load can be substituted by the load of other energy forms. And it is considered that the electric load and the heating load can substitute each other in this paper. The substitution relationship between them is expressed as:

$$\Delta P_t^{EFL,e}=-\xi_{e,h}\Delta P_t^{EFL,h} \tag{28}$$

$$\xi_{e,h}=\frac{\eta_e\lambda_e}{\eta_h\lambda_h} \tag{29}$$

where $\Delta P_t^{EFL,e}$ and $\Delta P_t^{EFL,h}$ are the alternative electric EFL and corresponding heating EFL, respectively; $\xi_{e,h}$ is the electrothermal substitution coefficient; η_e and η_h are the utilization efficiencies of electric energy and heat energy, respectively; and λ_e and λ_h are the calorific values of electric energy and heat energy, respectively.

III. Multi-objective Optimization Model of IESs and Solution Method

A. Objective Functions

The multi-objective optimization model of IES considering LDR under carbon emission trading mechanism aims to achieve the best economy and maximize the utilization of RES. The objective functions are established with the objectives of minimizing the total operating cost and the RES curtailment of IES.

1) Objective Function 1

The objective function of the minimum total operating cost can be expressed as:

$$\min f_1=C_{en}+C_{om}+C_{po}+C_{co_2} \tag{30}$$

where f_1 is the total operating cost; C_{en} is the cost of energy purchase; C_{om} is the cost of device maintenance; C_{po} is the cost of pollutant treatment; and C_{co_2} is the cost of carbon emission trading.

1) Cost of energy purchase

$$C_{en}=\sum_{t=1}^{T}c_{ele}P_t^{grid}+\frac{1}{\lambda_{gas}}\sum_{t=1}^{T}c_{gas}\left(\frac{P_t^{MT}}{\eta_{MT}}+\frac{H_t^{GB}}{\eta_{GB}}-P_t^{P2G}\eta_{P2G}\right) \tag{31}$$

where c_{ele} and c_{gas} are the purchase prices of electricity and natural gas, respectively.

2) Cost of device maintenance

$$C_{om}=\sum_{t=1}^{T}\left(\sum_{k=1}^{7}\phi_k P_t^k+C_t^{ES}\right) \tag{32}$$

where the values $1,2,...,7$ of k represent WT, PV, CHP, GB, P2G, HS, GS, respectively; P_t^k is the output power of device k; and ϕ_k is the maintenance cost coefficient of device k.

3) Cost of pollution treatment

In the operation process of IES, some pollutants will be produced, such as SO_2, NO_x, and inhalable particulate matter PM2.5. The pollutant emissions mainly come from CHP, GB, and power purchase. The pollutant treatment cost can be expressed as:

$$C_{po}=\sum_{t=1}^{T}\left(\varphi_{grid}P_t^{grid}+\varphi_{MT}P_t^{MT}+\varphi_{GB}H_t^{GB}\right) \tag{33}$$

where φ_{grid}, φ_{MT}, and φ_{GB} are the pollutant treatment costs per unit active power of electricity purchase, CHP, and GB, respectively.

2) Objective Function 2

The RES curtailment in IES is expressed by the difference between the maximum predicted output of RES and the actual RES accommodated by the system:

$$\min f_2 = \min \sum_{t=1}^{T} (P_t^{WT,ab} + P_t^{PV,ab}) = \min \sum_{t=1}^{T} (\left| P_t^{WT,\max} - P_t^{WT} \right| + \left| P_t^{PV,\max} - P_t^{PV} \right|) \quad (34)$$

where $P_t^{WT,ab}$ and $P_t^{PV,ab}$ are the wind power curtailment and PV power curtailment, respectively; $P_t^{WT,\max}$ and $P_t^{PV,\max}$ are the maximum predicted outputs of wind power and PV power, respectively; and P_t^{WT} and P_t^{PV} are the wind power and PV power accommodated by the system, respectively.

B. Constraint Conditions

1) Energy Balance Constraints

The energy balance constraints intend to ensure the balance between energy supply and consumption, as shown in (35)-(37).

1) Balance of electric power

$$P_t^{WT} + P_t^{PV} + P_t^{grid} + P_t^{MT} + P_t^{bat} = P_t^{load} + P_t^{P2G} + \Delta P_t^{TTL,e} + \Delta P_t^{QRL,e} + \Delta P_t^{EFL,e} \quad (35)$$

where P_t^{load} is the electric load of users; and $\Delta P_t^{TTL,e}$, $\Delta P_t^{QRL,e}$, and $\Delta P_t^{EFL,e}$ are the electric power variations of TTL, QRL, and EFL after LDR, respectively.

2) Balance of heat power

$$H_t^{HRB} + H_t^{GB} + H_t^{HS} = H_t^{heat} + \Delta P_t^{TTL,h} + \Delta P_t^{QRL,h} + \Delta P_t^{EFL,h} \quad (36)$$

where H_t^{heat} is the heating load of users; and $\Delta P_t^{TTL,h}$, $\Delta P_t^{QRL,h}$ and $\Delta P_t^{EFL,h}$ are the heat power variations of TTL, QRL, and EFL after LDR, respectively.

3) Balance of natural gas energy

$$F_t^{MT} + F_t^{GB} + Q_t^{GS} = F_t^{gas} + F_t^{P2G} \quad (37)$$

where F_t^{gas} is the natural gas purchased from the gas grid.

2) Equipment Operating Constraints

The equipment operating constraints are used to ensure the safe and stable operation of each device, as shown in (38)-(52).

1) Constraints of CHP

$$0 \le P_t^{MT} \le P^{MT,\max} \quad (38)$$

$$\left| P_t^{MT} - P_{t-1}^{MT} \right| \le r_{MT} \quad (39)$$

where $P^{MT,\max}$ is the upper limit output of MT; and r_{MT} is the maximum ramp rate of MT. It should be mentioned that (15) shows the relationship between electric power and heat power generated by CHP. Constraint (38) limits the upper/lower electric power output of MT. According to (15) and (38), the upper/lower limits of the heat power output of HRB can also be determined. Similarly, according to (15) and (39), the ramping up/down limits of HRB can also be determined.

2) Constraints of GB

$$0 \le H_t^{GB} \le H^{GB,\max} \quad (40)$$

$$\left| H_t^{GB} - H_{t-1}^{GB} \right| \le r_{GB} \quad (41)$$

where $H^{GB,\max}$ is the upper limit output of GB; and r_{GB} is the maximum ramp rate of GB.

3) Constraints of P2G

$$0 \le P_t^{P2G} \le P^{P2G,\max} \quad (42)$$

$$\left| P_t^{P2G} - P_{t-1}^{P2G} \right| \le r_{P2G} \quad (43)$$

where $P^{P2G,\max}$ is the maximum power of P2G; and r_{P2G} is the maximum ramp rate of P2G.

4) Constraints of ES

$$\frac{W^{bat,\min}}{C_r} \le SOC_t \le \frac{W^{bat,\max}}{C_r} \quad (44)$$

$$0 \le \left| P_t^{bat} \right| \le P^{bat,\max} \quad (45)$$

where $W^{bat,\max}$ and $W^{bat,\min}$ are the maximum and minimum ES capacities of the battery, respectively; and $P^{bat,\max}$ is the maximum output power of the battery.

Besides, to prevent the battery from being charged and discharged simultaneously, the following condition should be met:

$$P_t^{bat,c} P_t^{bat,d} = 0 \quad (46)$$

5) Constraints of HS and GS

$$W^{HS,\min} \le W_t^{HS} \le W^{HS,\max} \quad (47)$$

$$0 \le \left| H_t^{HS} \right| \le H^{HS,\max} \quad (48)$$

$$W^{GS,\min} \le W_t^{GS} \le W^{GS,\max} \quad (49)$$

$$0 \le \left| Q_t^{GS} \right| \le Q^{GS,\max} \quad (50)$$

where $W^{HS,\max}$ and $W^{HS,\min}$ are the maximum and minimum HS capacities, respectively; $W^{GS,\max}$ and $W^{GS,\min}$ are the maximum and minimum GS capacities, respectively; and $H^{HS,\max}$ and $Q^{GS,\max}$ are the maximum output power of HS and GS, respectively.

In addition, HS and GS both cannot release energy and store energy at the same time, thus the following constraints should also be satisfied:

$$H_t^{ch} H_t^{dis} = 0 \quad (51)$$

$$Q_t^{ch} Q_t^{dis} = 0 \quad (52)$$

3) Tie Line Constraints

The tie line constraints limit the maximum power exchange between the system and the grid.

$$0 \le P_t^{grid} \le P^{grid,\max} \quad (53)$$

where $P^{grid,\max}$ is the maximum electricity purchased from the power grid.

4) LDR Model Constraints

The LDR model constraints are used to ensure users' basic energy demands and enhance their satisfaction with energy use.

$$0 \le \left| \Delta P_t^{TTL} \right| \le \Delta P^{TTL,\max} \quad (54)$$

$$0 \le \left| \Delta P_t^{QRL} \right| \le \Delta P^{QRL,\max} \quad (55)$$

$$0 \le \left| \Delta P_t^{EFL} \right| \le \Delta P^{EFL,\max} \quad (56)$$

where $\Delta P^{TTL,\max}$, $\Delta P^{QRL,\max}$, and $\Delta P^{EFL,\max}$ are the upper limits of TTL, QRL, and EFL, respectively.

It should be mentioned that in this paper, we mainly consider the influence of ladder-type carbon emission trading mechanism and refined LDR strategies on IES operation. For the uncertainties of RES and load, since the IES in this paper is connected to the external power grid, some uncertainties of RES output and load demand can be smoothed through the power exchange between IES and power grid. In addition, the refined LDR model is considered in the optimal scheduling of IES. When the fluctuations of RES genera-

tion and load demand occur, the LDR model can transfer, reduce, or replace part of the load, so as to fully utilize RES and satisfy the energy demand of users. Thus the partial adverse influence of the uncertainties can also be eliminated by the LDR model.

C. Solution Method

In multi-objective optimization problems, each objective function conflicts with each other, and it is impossible to achieve optimal results for multiple objectives simultaneously. So the optimal solution of multi-objective optimization problem is a set of solutions in which the value of any objective function cannot be further optimized without deteriorating other objective functions, i. e., the Pareto optimal solution set.

In this paper, the niche multi-objective particle swarm optimization (NMOPSO) algorithm is applied to solve the multi-objective problem of IES. The algorithm uses niche sharing mechanism to update the position of particles and maintain the diversity of solutions and the uniformity of distribution. And the chaotic mutation is introduced to disturb some non-dominant particles in a small range, which improves the global search ability of the algorithm and avoids falling into local optimization. Compared with other multi-objective optimization algorithms, the NMOPSO algorithm has been verified to have better performance in terms of computational efficiency and accuracy [24]. The Pareto optimal solution set can be converged quickly by NMOPSO algorithm, and the diversity of solutions also can be ensured at the same time, so that the Pareto set contains the optimal solutions of multiple optimization objectives in different situations. Figure 2 shows the flow chart of NMOPSO algorithm for solving multi-objective optimization problem in IES.

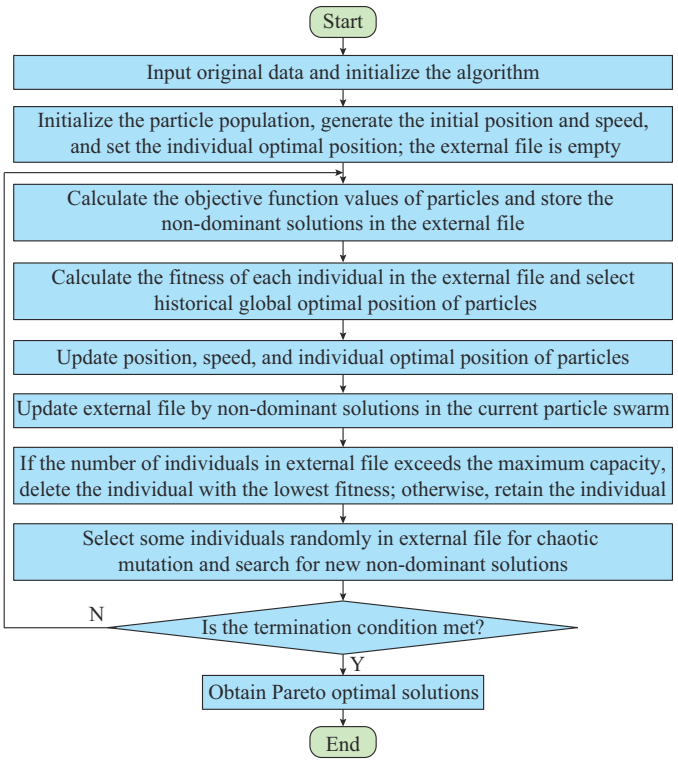

Fig. 2. Flow chart of NMOPSO algorithm.

IV. Case Study

A. Parameter Setting

The data of electric and heating loads and the wind and PV power output come from a typical day of Northeast China. The simulation parameters are listed in Table I and Table II. And the predicted electric load, heat load, and the maximum outputs of wind and PV power are shown in Fig. 3. The time-sharing price of electricity purchased from the power grid is shown in Fig. 4. The price of natural gas purchased from the gas grid is 2.83 ¥/m^3. Before considering LDR, the initial price of electricity sold by the IES to users is 0.78 ¥/kWh and the price of heat energy sold is 0.37 ¥/kWh. The proportions of TTL, QRL, EFL, and UL in the total load are 20%, 20%, 10%, and 50%, respectively. The simulations are carried out on a PC with AMD Ryzen 7-5700U, 1.80 GHz and 16 GB RAM. The simulation environment is MATLAB R2016a.

TABLE I
Parameters of IES Model

Parameter	Value	Parameter	Value	Parameter	Value
c_{bat}	0.413 ¥/kWh	F_{co_2}	280 ¥/t	γ	0.5
ε_p	424 g/kWh	V_r	60 V	ρ	0.25
δ	6 MJ/kWh	C_r	210 kWh	η_{P2G}	0.7
ε_h	0.102 t/GJ	d	100 kg	η_{ch}	0.9
ε_e	968 g/kWh	η_{MT}	0.35	η_{dis}	0.85
ε_g	220 g/m^3	η_{HRB}	0.85	μ_{ch}	0.9
λ_{gas}	9.78 kWh/m^3	η_{GB}	0.9	μ_{dis}	0.85

TABLE II
Parameters of IES Constraints

Parameter	Value	Parameter	Value	Parameter	Value
$P^{MT,\max}$	100 kW	$P^{grid,\max}$	100 kW	$P^{P2G,\max}$	60 kW
$P^{bat,\max}$	100 kW	$H^{HS,\max}$	100 kW	$Q^{GS,\max}$	50 kW
$W^{bat,\max}$	200 kWh	$W^{HS,\max}$	400 kWh	$W^{GS,\max}$	150 kWh
$W^{bat,\min}$	40 kWh	$Q^{QB,\max}$	300 kW	r_{P2G}	5 kW/min
r_{GB}	15 kW/min	r_{MT}	10 kW/min		

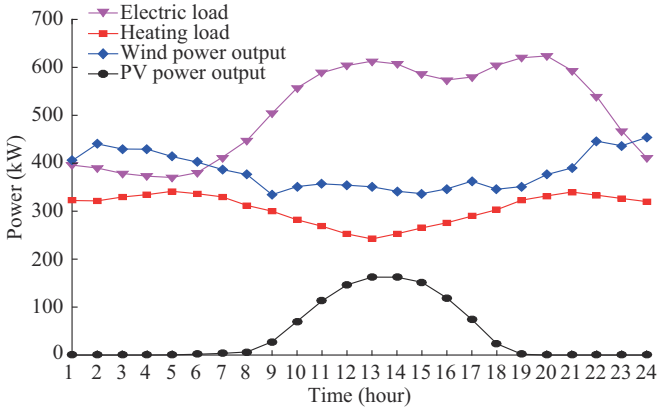

Fig. 3. Predicted electric load, heating load, and the maximum outputs of wind power and PV power.

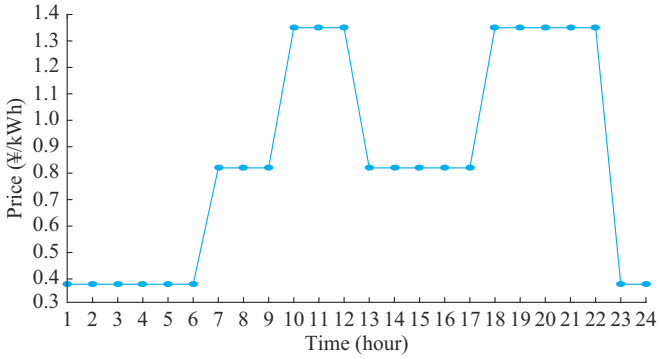

Fig. 4. Time-sharing price of electricity purchased from power grid.

B. Analysis of Simulation Results

1) Pareto Optimal Solutions

The Pareto frontier solution set calculated by NMOPSO algorithm is shown in Fig. 5. In order to ensure the solution accuracy, this paper makes a trade-off between computation accuracy and computation time, and the computation time of the NMOPSO algorithm for solving the proposed multi-objective optimization problem is 41.26 s.

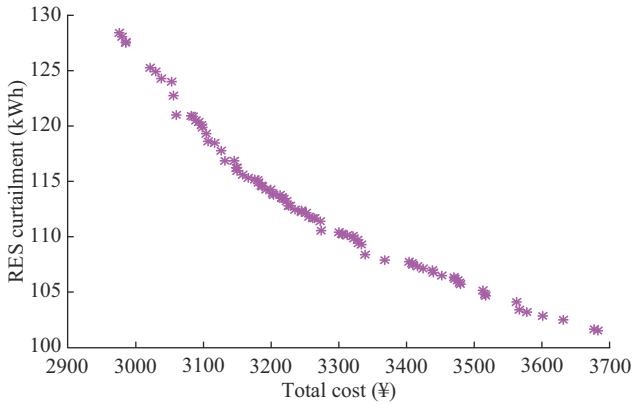

Fig. 5. Pareto frontier solution set.

It can be observed from Fig. 5 that if economic benefits are given priority, the operating cost reaches the lowest, which is ¥2975.34, but the RES curtailment is the highest at this time, reaching 128.39 kWh. When the improvement of RES utilization rate is given priority, the minimum RES curtailment is 101.49 kWh, but the operating cost is the highest, which is up to ¥3682.06. In practical application, it is necessary to comprehensively weigh the two objective functions and scientifically determine the optimal operation scheme of IES according to the expectations and requirements of decision-makers. Therefore, the decision-makers must choose the optimal compromise solution from a set of Pareto optimal solutions.

In order to determine the scheme that is closest to the optimal level, i. e., both objective functions are minimized, the technique for order preference by similarity to an ideal solution (TOPSIS) decision-making method is used to select the only compromise scheme. By TOPSIS decision-making method, the proximity index between each solution and the optimal level can be obtained, and sorted in descending order. And the greater the proximity index, the closer to the optimal level [25].

For the Pareto frontier solution sets in various scenarios, the operating costs and RES curtailment are assumed to have the same weight in this paper. And the first six solutions of Pareto set determined by TOPSIS decision-making method are shown in Table III. The solution 1 is regarded as the best compromise scheme.

TABLE III
FIRST SIX SOLUTIONS OF PARETO SET DETERMINED BY TOPSIS DECISION-MAKING METHOD

Order	Total cost (¥)	RES curtailment (kWh)	Proximity index
1	3273.96	110.536	0.62070
2	3235.83	112.419	0.61189
3	3225.65	112.812	0.61107
4	3338.55	108.356	0.61083
5	3255.40	111.811	0.61014
6	3228.82	112.773	0.60972

2) Scenario Comparison

In order to research the impacts of LDR and carbon emission trading mechanism built in this paper, this part sets up four different scenarios. Similarly, for the Pareto frontier solution set in each scenario, the TOPSIS decision-making method is adopted to determine the only compromise scheme.

Scenario 1: the unified carbon emission cost calculation model [26] is used in the optimal scheduling of IES, but LDR is not considered.

Scenario 2: the unified carbon emission cost calculation model is used in the optimal scheduling of IES, and LDR is also considered.

Scenario 3: the ladder-type carbon emission cost calculation model based on rewards and penalties is used in the optimal scheduling of IES, but LDR is not considered.

Scenario 4: the ladder-type carbon emission cost calculation model based on rewards and penalties is used in the optimal scheduling of IES, and LDR is also considered.

The simulation results of the four scenarios are shown in Table IV. From Table IV, it can be observed that compared with scenarios 1 and 3 that do not consider LDR, for scenarios 2 and 4, the total operating costs are reduced by ¥150.48 and ¥141.4, respectively, and the RES curtailments are reduced by 153.135 kWh and 137.644 kWh, respectively. Besides, the other costs are also reduced to varying degrees. This is because after participating in LDR, the users change their energy consumption patterns, transfer part of load to the period of low energy price, and reduce a certain amount of load. At the same time, the electric load and heating load can be replaced by lower-cost load form. From the above comparison results, it can be observed that by considering the refined LDR model, the operating costs and RES curtailment of IES can be significantly reduced. The economic benefits of IES can be greatly improved, and the RES can also be fully utilized, which verifies the effectiveness of the LDR model proposed in this paper.

TABLE IV
SIMULATION RESULTS OF FOUR SCENARIOS

Scenario	Total operating cost (¥)	Device maintenance cost (¥)	Energy purchase cost (¥)	Carbon trading cost (¥)	Carbon emission (kg)	Pollution treatment cost (¥)	RES curtailment (kWh)	Rate of RES curtailment (%)
1	3502.62	369.18	2437.72	252.20	2337.85	443.52	268.486	2.63
2	3352.14	348.24	2337.65	237.76	2285.74	428.49	115.351	1.13
3	3415.43	368.32	2420.86	195.71	2238.23	430.54	248.180	2.41
4	3273.96	352.16	2316.52	188.17	2201.46	417.11	110.536	1.08

It can also be observed from Table IV that compared with scenarios 1 and 2 that use the unified carbon emission cost calculation model, the carbon emissions of scenarios 3 and 4 are reduced by 99.62 kg and 84.28 kg, respectively, and the carbon emission trading costs are reduced by ¥56.49 and ¥49.59, respectively. Besides, the total operating cost and the RES curtailment in scenario 3 are also lower than those in scenario 1. Similarly, the same is true for scenario 4 compared with scenario 2. It can be known that compared with the unified carbon emission cost calculation model, using the ladder-type carbon emission cost calculation model based on rewards and penalties is more effective in reducing the carbon emissions and carbon emission trading cost of IES. Therefore, the ladder-type carbon emission trading mechanism proposed in this paper can not only strictly control the carbon emissions, but also effectively decrease the carbon emission trading expenses.

Figure 6 shows the initial and time-sharing prices of energy purchased by users from IES before and after considering LDR. From Fig. 6(a), it can be observed that the peak period of electricity price is mainly in 10:00-12:00 and 20:00-22:00, and the valley period is mainly in 01:00-07:00. And from Fig. 6(b), it can be observed that the peak period of heat price is mainly in 11:00-14:00 and 20:00-22:00, while the valley period is mainly in 01:00-07:00 and 18:00-19:00.

The electric load curve and heating load curve before and after considering LDR and the corresponding changes of various types of loads are shown in Fig. 7(a) and (b), respectively.

As can be observed that part of the electric TTL in the high electricity price period, i.e., 10:00-12:00 and 20:00-22:00, is transferred to the low electricity price period. And part of the heating TTL in the high heat price period, i.e., 11:00-14:00 and 20:00-22:00, is transferred to the low heat price period. Meanwhile, it also can be observed that some electric QRL is reduced in the high electricity price period, i.e., 10:00-12:00 and 20:00-22:00. And some heating QRL is also reduced in the high heat price period, i.e., 13:00-14:00. Besides, part of electric EFL is converted into heating load in high electricity price period, i.e., 10:00-12:00 and 20:00-22:00, and low heat price period, i.e., 08:00-10:00, 15:00-19:00, and 23:00-24:00. In low electricity price period, i.e., 15:00-19:00, and high heat price period, i.e., 11:00-12:00 and 20:00-22:00, part of the heating EFL is converted into electric load. So by considering LDR, the energy load are effectively adjusted to make the overall daily load curve of users consistent with the output of RES.

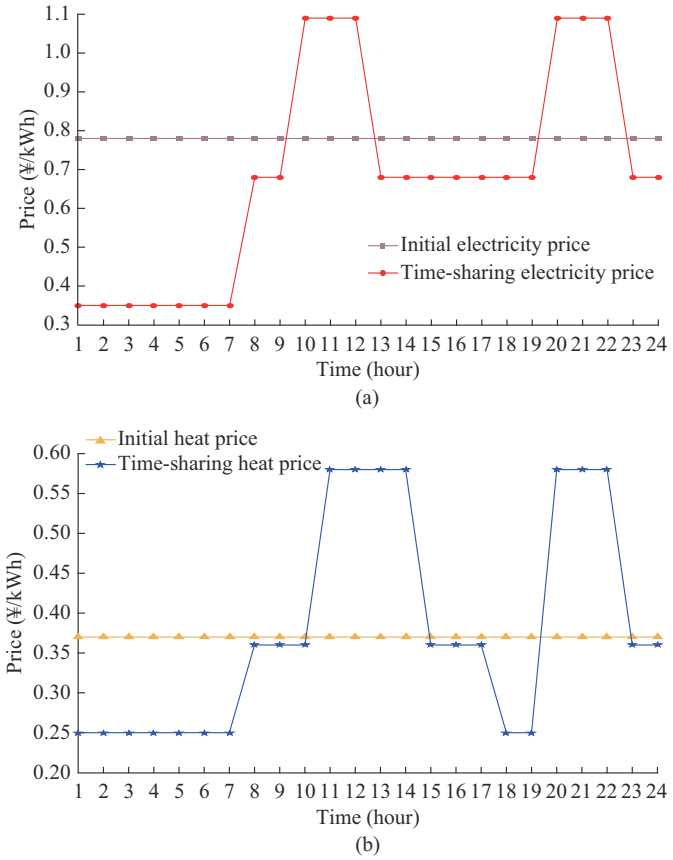

Fig. 6. Initial and time-sharing energy prices. (a) Initial and time-sharing electricity prices. (b) Initial and time-sharing heat prices.

Figures 8 and 9 show the electric and heat power balance in scenario 4, where ES-CH and ES-DCH represent ES charge and discharge, respectively; and HS-CH and HS-DCH represent HS charge and discharge, respectively. From Fig. 8, it can be observed that in 01:00-12:00 and 22:00-24:00, since the electric demand of users is relatively small, the electric demand is mainly met by the output of CHP, WT, and PV, and the remaining electric energy is supplied to P2G or stored by ES. In 13:00-21:00, as the electric demand is in the peak period, the electric demand is not only met by the output of CHP, WT, and PV, but also needs to be met by the ES discharge and the electricity purchased from the grid. From Fig. 9, it can be observed that in 05:00-22:00, the heating demand is mainly met by the heat from CHP and GB. In 01:00-04:00 and 23:00-24:00, since the heating demand is great, the heating demand is not only met by CHP and GB, but also needs to be met by HS heat release.

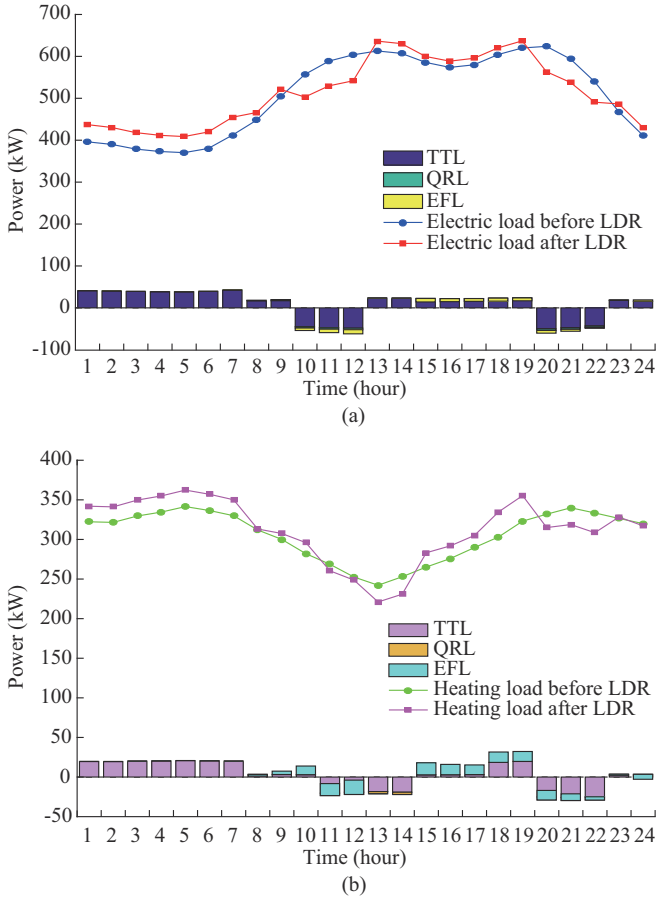

Fig. 7. Variations of load before and after considering LDR. (a) Variations of electric load. (b) Variations of heating load.

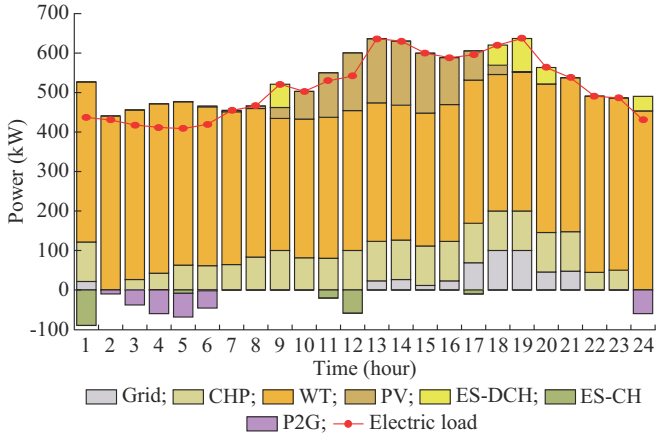

Fig. 8. Electric power balance in scenario 4.

Figures 10 and 11 show the electric and heat power balances in scenario 3, respectively. Since LDR is not considered in scenario 3, the electric and heating loads are both original loads without peak load shifting. The output of each device is also affected by the original load during the scheduling cycle, which causes an increase in the operating cost, and the ability to accommodate RES is also decreased.

Figure 12 shows the comparison of RES accommodation of scenarios 3 and 4 in the scheduling cycle. It can be observed that the RES curtailment mainly occurs in 03:00-06:00 in scenario 4. And the RES curtailment mainly occurs in 01:00-07:00 and 23:00-24:00 in scenario 3. It is obvious that the RES curtailment in scenario 4 is less than that in scenario 3, which verifies that taking LDR into account in the optimal scheduling of IES can significantly promote the utilization of RES.

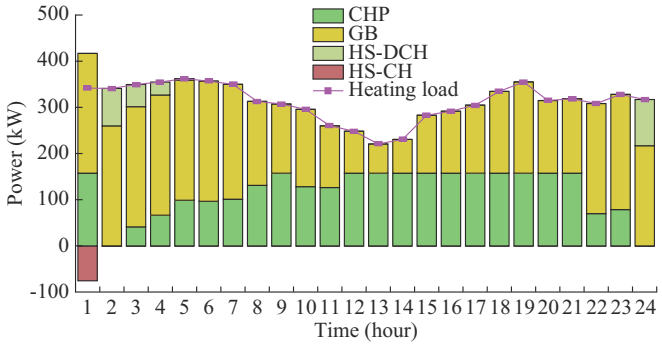

Fig. 9. Heat power balance in scenario 4.

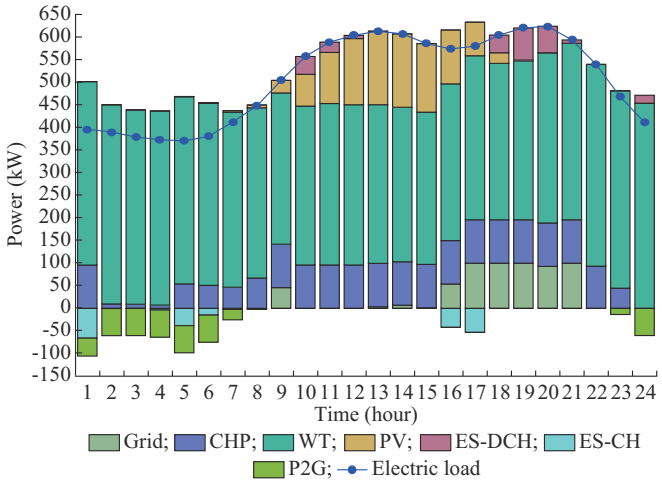

Fig. 10. Electric power balance in scenario 3.

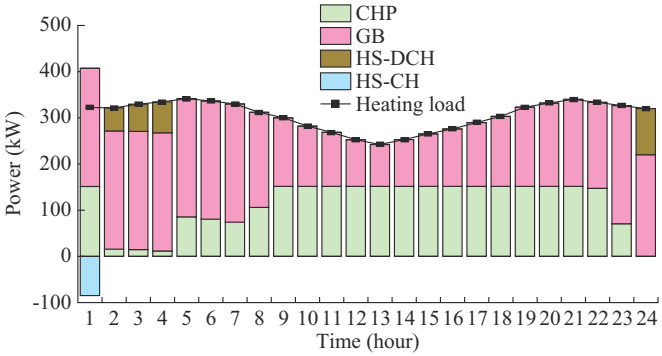

Fig. 11. Heat power balance in scenario 3.

3) Impact Analysis of LDR Under Different Load Types

In the above research, the proportion of all kinds of loads involved in LDR is assumed to be fixed. But in practical application, due to different electricity and heat consumption habits of users, the impact of LDR on the IES operation is also different. In order to research the above effects, three scenarios are set as follows.

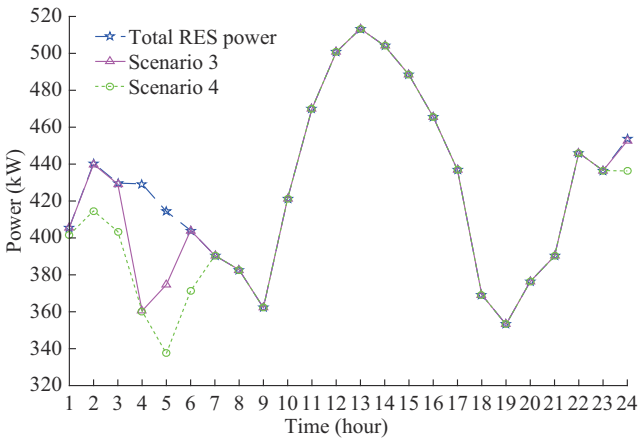

Fig. 12. Comparison of RES accommodation in scenarios 3 and 4.

Scenario 5: LDR is acted by PDL alone.

Scenario 6: LDR is acted by EFL alone.

Scenario 7: LDR is jointly acted by PDL and EFL.

It is assumed that the proportions of UL and CL in the total load are fixed in the following analysis, both 50% and 50%. And for PDL, the ratio of TTL to QRL is 1:1. The effects of LDR under different load types on IES operation are shown in Table V. The improvement rates of each scenario are also given in Table V compared with the situation without considering LDR.

TABLE V
EFFECTS OF LDR UNDER DIFFERENT LOAD TYPES ON IES OPERATION

Scenario	Total cost (¥)	Improvement rate of total cost (%)	RES curtailment (kWh)	Improvement rate of RES curtailment (%)
5	3317.15	2.88	135.28	45.49
6	3366.36	1.43	172.58	30.46
7	3273.96	4.14	110.54	55.46

From Table V, it can be observed that the effects of different load types participating in LDR are different. Ranking based on the improvement rate of objective function values, the IES yields the lowest benefit when LDR is acted by EFL alone, followed by PDL alone. The greatest benefit is achieved through the joint action of EFL and PDL. The main reason is that when LDR is only acted by single load type, the flexible regulation capability of LDR cannot be fully played due to the constraints of various devices and energy supply side. But when two types of load work together, the complementary response characteristics of different types of LDR resources can be fully utilized, and the system can simultaneously control the time and form of load energy consumption, so the economy and the RES utilization can be effectively improved.

In addition, in order to study the influence of electric LDR and heating LDR in IES, three other scenarios are set as follows:

Scenario 8: LDR is acted on by electric load alone.

Scenario 9: LDR is acted on by heating load alone.

Scenario 10: LDR is jointly acted by electric load and heating load.

The effects of LDR under different load forms on IES operation are shown in Table VI. From Table VI , it can be observed that the benefits of scenarios 8 and 9 are worse than that of scenario 10. The reason is that when only a single load form participates in LDR, the energy consumption time and the quantity of other load forms cannot be adjusted. Besides, the conversion between different load forms involved in LDR has also changed from two-way to one-way. All these make the benefit of single-load form response worse than that of multi-load form response.

TABLE VI
EFFECTS OF LDR UNDER DIFFERENT LOAD FORMS ON IES OPERATION

Scenario	Total cost (¥)	Improvement rate of total cost (%)	RES curtailment (kWh)	Improvement rate of RES curtailment (%)
8	3343.41	2.11	129.83	47.68
9	3382.62	0.96	156.88	36.78
10	3273.96	4.14	110.54	55.46

V. CONCLUSION

In order to promote the development of low-carbon economy and the utilization of RES in multi-energy coupling systems, an innovative multi-objective optimization model of IES considering the ladder-type carbon emission trading mechanism and the refined LDR strategies is proposed. According to the simulation results, the conclusions are as follows.

1) On the premise of guaranteeing the economic operation of IES, considering LDR can improve the utilization efficiency of RES and play a positive role in environmental protection.

2) Compared with the unified carbon emission cost calculation model, the ladder-type carbon emission cost calculation model based on rewards and penalties can significantly reduce the carbon emissions and carbon trading cost, and has a better effect on the economy of IES.

3) The contributions of LDR to IES are influenced by many factors. Under the same conditions, the more diversified the load types and load forms involved in LDR, the better the effect of implementing LDR.

In the future work, the uncertainties of renewable energy and load demand will be considered in system operation via some methods such as scenario-based stochastic programming and adaptive dynamic programming. Besides, we plan to establish detailed models of power, heat, and gas system based on the characteristics and coupling relationships of different energy networks, and consider their network models and flow constraints in the optimal operation.

REFERENCES

[1] J. Li, G. Li, S. Ma *et al*., "Modeling and simulation of hydrogen energy storage system for power-to-gas and gas-to-power systems," *Journal of Modern Power Systems and Clean Energy*, vol. 11, no. 3, pp. 885-895, May 2023.

[2] Y. Luo, H. Yuan, Z. Hu *et al*., "Optimal scheduling of micro-energy grid based on Pareto frontier under uncertainty and pollutant emissions," *IEEE Transactions on Smart Grid*, doi: 10.1109/

TSG.2023.3273816
[3] H. Hao, Y. Luo, and D. Yang, "Real-time optimization for microgrid energy scheduling based on approximate dynamic programming," in *Proceedings of 2022 4th International Conference on Smart Power & Internet Energy Systems* (*SPIES*), Beijing, China, Dec. 2022, pp. 2301-2306.
[4] Z. Xu, G. Han, L. Liu *et al*., "Multi-energy scheduling of an industrial integrated energy system by reinforcement learning-based differential evolution," *IEEE Transactions on Green Communications and Networking*, vol. 5, no. 3, pp. 1077-1090, Sept. 2021.
[5] V. H. Bui, A. Hussain, Y. H. Im *et al*., "An internal trading strategy for optimal energy management of combined cooling, heat and power in building microgrids," *Applied Energy*, vol. 239, pp. 536-548, Apr. 2019.
[6] X. Chen, M. B. McElroy, and C. Kang, "Integrated energy systems for higher wind penetration in China: formulation, implementation, and impacts," *IEEE Transactions on Power Systems*, vol. 33, no. 2, pp. 1309-1319, Mar. 2018.
[7] D. Zhang, Y. Hu, and Y. Gao, "Flexibility improvement of CHP unit for wind power accommodation," *Journal of Modern Power Systems and Clean Energy*, vol. 10, no. 3, pp. 731-742, May 2022.
[8] J. Hu, X. Liu, M. Shahidehpour *et al*., "Optimal operation of energy hubs with large-scale distributed energy resources for distribution network congestion management," *IEEE Transactions on Sustainable Energy*, vol. 12, no. 3, pp. 1755-1765, Jul. 2021.
[9] Z. Wang, Y. Shi, Y. Tang *et al.*, "Low carbon economy operation and energy efficiency analysis of integrated energy systems considering LCA energy chain and carbon trading mechanism," *Proceedings of the CSEE*, vol. 39, no. 6, pp. 1614-1626, Mar. 2019.
[10] Y. Luo, X. Zhang, D. Yang *et al*., "Emission trading based optimal scheduling strategy of energy hub with energy storage and integrated electric vehicles," *Journal of Modern Power Systems and Clean Energy*, vol. 8, no. 2, pp. 267-275, Mar. 2020.
[11] Y. Luo, D. Yang, Z. Yin *et al*., "Optimal configuration of hybrid-energy microgrid considering the correlation and randomness of the wind power and photovoltaic power," *IET Renewable Power Generation*, vol. 14, no. 4, pp. 616-627, Mar. 2020.
[12] X. Zhang, X. Liu, J. Zhong *et al*., "Electricity-gas-integrated energy planning based on reward and penalty ladder-type carbon trading cost," *IET Generation*, *Transmission & Distribution*, vol. 13, no. 23, pp. 5263-5270, Dec. 2019.
[13] T. Qin, H. Liu, J. Wang *et al.*, "Carbon trading based low-carbon economic dispatch for integrated electricity-heat-gas energy system," *Automation of Electric Power Systems*, vol. 42, no. 14, pp. 8-13, Jul. 2018.
[14] Y. Luo, H. Hao, D. Yang *et al*., "Optimal operation strategy of combined heat and power system considering demand response and household thermal inertia," *IEEE Transactions on Consumer Electronics*, vol. 69, no. 3, pp. 366-376, Aug. 2023.
[15] P. Harsh and D. Das, "Optimal coordination strategy of demand response and electric vehicle aggregators for the energy management of reconfigured grid-connected microgrid," *Renewable and Sustainable Energy Reviews*, vol. 160, p. 112251, May 2022.
[16] Y. Luo, X. Zhang, D. Yang *et al*., "Optimal operation and cost-benefit allocation for multi-participant cooperation of integrated energy system," *IET Generation*, *Transmission & Distribution*, vol. 13, no. 22, pp. 5239-5247, Nov. 2019.
[17] M. K. Kiptoo, M. E. Lotfy, O. B. Adewuyi *et al*., "Integrated approach for optimal techno-economic planning for high renewable energy-based isolated microgrid considering cost of energy storage and demand response strategies," *Energy Conversion and Management*, vol. 215, p. 112917, Jul. 2020.
[18] C. Shao, Y. Ding, J. Wang *et al.*, "Modeling and integration of flexible demand in heat and electricity integrated energy system," *IEEE Transactions on Sustainable Energy*, vol. 9, no. 1, pp. 361-370, Jan. 2018.
[19] W. Wang, S. Huang, G. Zhang *et al*., "Optimal operation of an integrated electricity-heat energy system considering flexible resources dispatch for renewable integration," *Journal of Modern Power Systems and Clean Energy*, vol. 9, no. 4, pp. 699-710, Jul. 2021.
[20] T. A. Nguyen, "Optimization in microgrid design and energy management," Ph.D. dissertation, Department of Electrical Engineering, Missouri University of Science and Technology, Rolla, Missouri, USA, 2014.
[21] T. A. Nguyen and M. L. Crow, "Stochastic optimization of renewable-based microgrid operation incorporating battery operating cost," *IEEE Transactions on Power Systems*, vol. 31, no. 3, pp. 2289-2296, May 2016.
[22] H. A. Kiehne, *Battery Technology Handbook*. Boca Raton: CRC Press, 2003.
[23] O. Tremblay and L. A. Dessaint, "Experimental validation of a battery dynamic model for EV applications," *World Electric Vehicle Journal*, vol. 3, no. 2, pp. 289-298, Jun. 2009.
[24] W. Liu, C. Xie, J. Wen *et al*., "Optimization of transmission network maintenance scheduling based on niche multi-objective particle swarm algorithm," *Proceedings of the CSEE*, vol. 33, no. 4, PP. 141-148, Feb. 2013.
[25] H. Allouhi, A. Allouhi, and A. Jamil, "Multi-objective optimization of a CSP-based dish Stirling field layout using genetic algorithm and TOPSIS method: case studies in Ouarzazate and Madrid," *Energy Conversion and Management*, vol. 254, p. 115220, Feb. 2022.
[26] Z. Wei, S. Zhang, G. Sun *et al*., "Carbon trading based low-carbon economic operation for integrated electricity and natural gas energy system," *Automation of Electric Power Systems*, vol. 40, no. 15, pp. 9-16, Aug. 2016.

Yanhong Luo received the B.S. degree in automation control and the Ph.D. degree in control theory and control engineering from Northeastern University, Shenyang, China, in 2003 and 2009, respectively. She is currently with Northeastern University as a Professor. Her research interests include distributed control and optimal operation of energy internet, adaptive dynamic programming, data-driven self-learning control and its industrial applications.

Haowei Hao received the B.S. degree from Shanghai University of Engineering Science, Shanghai, China, in 2021, and he is currently working toward the M.S. degree in the Department of Electric Engineering, Northeastern University, Shenyang, China. His research interests include optimal operation of integrated energy system, clean energy utilization, and demand response.

Dongsheng Yang received the B.S. degree in testing technology and instrumentation, the M.S. degree in power electronics and electric drives, and the Ph.D. degree in control theory and control engineering from Northeastern University, Shenyang, China, in 1999, 2004, and 2007, respectively. He is currently a Professor with Northeastern University. His current research interests include multi-energy power system, distributed generation, and artificial intelligence-based fault diagnosis and protection.

Bowen Zhou received the B.Sc. and M.Sc. degrees from Wuhan University, Wuhan, China, in 2010 and 2012, respectively, and the Ph.D. degree from Queen's University Belfast, Belfast, UK, in 2016, all in electrical engineering. He is currently with Northeastern University as an Associate Professor. His research interests include energy system operation, energy storage, and energy internet.